Journal of Power Sources 225 (2013) 141–149

Contents lists available at SciVerse ScienceDirect

Journal of Power Sources

journal homepage: www.elsevier.com/locate/jpowsour

Glycerol electro-oxidation on a carbon-supported platinum catalyst at intermediate temperatures

Keisuke Ishiyama, Fumihiko Kosaka, Iori Shimada, Yoshito Oshima, Junichiro Otomo*

Department of Environment Systems, Graduate School of Frontier Sciences, The University of Tokyo, 5-1-5 Kashiwanoha, Kashiwa, Chiba 277-8563, Japan

HIGHLIGHTS

- A high oxidation current in glycerol electro-oxidation was observed at 250 °C.
- High selectivity for CO_2 production was obtained at 250 °C.
- C–C bond dissociation ratio reached 70–80% at both low and high potentials.
- Stable operation during glycerol electro-oxidation at around 250 °C requires a high S/C ratio.
- The present observations provide strategies for the effective operation of DAFCs.

ARTICLE INFO

Article history:
Received 17 July 2012
Received in revised form
28 September 2012
Accepted 12 October 2012
Available online 23 October 2012

Keywords:
Electro-oxidation
Glycerol
Direct alcohol fuel cell
Intermediate temperature
Cesium dihydrogen phosphate

ABSTRACT

The electro-oxidation of glycerol on a carbon-supported platinum catalyst (Pt/C) in combination with a reaction products analysis was investigated at intermediate temperatures (235–260 °C) using a single cell with a CsH_2PO_4 proton conducting solid electrolyte. A high current density was achieved. The main products were H_2, CO_2 and CO but the formation of C2 compounds, such as glycolic acid and ethane, was also observed. In addition, several C3 compounds were detected as minor products. A reaction products analysis revealed that the C–C bond dissociation ratio of glycerol was 70–80% at both low and high potentials (>200 mV *vs.* reversible hydrogen electrode) at 250 °C, suggesting that rapid dissociation occurs on Pt/C. The reaction products analysis also suggested that hydrogen production *via* thermal decomposition and/or steam reforming of glycerol (indirect path) and direct electro-oxidation of glycerol (direct path) proceed in parallel. More detailed reaction paths involving C1, C2 and C3 reaction products are discussed as well as the possible rate-determining step in glycerol electro-oxidation at intermediate temperatures.

1. Introduction

Development of new power generation technology and relevant alternative fuels are increasingly important issues in the search for feasible ways to address the growth in global energy demand. A direct alcohol fuel cell (DAFC), which can adapt to diverse fuels, is an effective energy conversion technology for generating electricity from various small organic molecules. Currently, glycerol is attracting considerable attention because it is obtained as a by-product of biodiesel production [1] and, because annual biodiesel production is expected to increase, the production of glycerol may exceed demand. Therefore, possible uses for the excess amount of glycerol should be investigated. Glycerol has a high energy density (6.26 kWh L^{-1}) and is also non-toxic, non-flammable, and non-volatile, which are ideal properties for a wide variety of power applications [2].

The electro-oxidation of glycerol has been investigated at relatively low temperatures in acidic media [3–9], alkaline media [3,9–12] and at near neutral pH [13]. The previous studies indicate that glycerol is not completely oxidized to CO_2 at around room temperature in either acidic or alkaline media because of slow electro-oxidation kinetics and the high energy barrier for C–C bond dissociation. A recent differential electrochemical mass spectroscopic (DEMS) study of glycerol electro-oxidation on platinum in an H_2SO_4 solution found that the contribution of CO_2 formation to the overall Faradaic current (i.e., CO_2 current efficiency) was only about 3–5% at around 600–700 mV [6]. The formation of partial oxidation products (C3 products) such as glyceraldehyde and glyceric acid has also been reported by means of DEMS [6] and liquid chromatography [3] in an acetic medium.

* Corresponding author. Tel.: +81 4 7136 4714; fax: +81 4 7136 4715.
E-mail address: otomo@k.u-tokyo.ac.jp (J. Otomo).

0378-7753/$ – see front matter © 2012 Elsevier B.V. All rights reserved.
http://dx.doi.org/10.1016/j.jpowsour.2012.10.035

In addition, glycerol electro-oxidation involves the formation of surface-bonded CO in both acidic [6] and alkaline media [10,12]. Those results suggest that C–C bond dissociation and subsequent oxidation of adsorbed CO may determine the reaction rate and selectivity during glycerol electro-oxidation.

To achieve total oxidation of glycerol to CO_2 and accelerate the rate of electro-oxidation, one effective means is to raise the reaction temperature. Recently, we reported electro-oxidation of C2 alcohols, ethanol and ethylene glycol, on carbon supported platinum (Pt/C) at around 250 °C [14,15], wherein the dominant products from ethanol were CO_2 and CH_4 and those for ethylene glycol were CO_2 and CO. Furthermore, the C–C bond dissociation ratio was found to be higher than 90% [14] and 95% [15] for ethanol and ethylene glycol, respectively. At an intermediate temperature of about 250 °C, therefore, activation of the dominant reaction steps in glycerol electro-oxidation, such as C–C bond dissociation and subsequent oxidation of adsorbates, would be expected. Improvements of slow kinetics and incomplete total oxidation of glycerol will provide a strategy for the effective use of a variety of alcohol fuels in DAFCs.

This work is the first report on the electro-oxidation of glycerol (C3 polyalcohol) on Pt/C at intermediate temperatures (235–260 °C), performed with an intermediate temperature fuel cell (ITFC) using a proton conducting oxyacid solid electrolyte, cesium dihydrogen phosphate (CDP: CsH_2PO_4). CDP has a high proton conductivity at intermediate temperatures ($>10^{-2}$ S cm^{-1} at 250 °C) under an appropriate humidified condition [16–18]. To understand the mechanism of glycerol electro-oxidation at intermediate temperatures, we conducted an analysis of reaction products and electrode kinetics. Because glycerol oxidation involves C1, C2 and C3 reaction products, the reaction route may be more complex than for C1 and C2 alcohols such as methanol, ethanol and ethylene glycol: (1) Glycerol → partially oxidized C3 products; (2) Glycerol → C1 + C2 products after C–C bond dissociation; (3) hydrogen production *via* thermal decomposition and steam reforming of glycerol. In this study, we attempted to detect C1, C2 and C3 carbonaceous species formed during glycerol electro-oxidation by gas and liquid chromatography. The results provide new insights into polyalcohol electro-oxidation mechanism and demonstrate the advantages of DAFCs operating at intermediate temperatures.

2. Experimental

2.1. Preparation of the single cell

Electrochemical measurements of glycerol electro-oxidation in the gas phase were performed with a single cell fabricated with a Pt/C electrode and CsH_2PO_4 solid electrolyte. Fabrication procedure of the single cell followed that described in our previous studies [14,15,19]. A Pt/C electrode was prepared from a commercial carbon-supported platinum catalyst (Pt/C, 46 wt%-Pt, Tanaka Kikinzoku Kogyo, Japan). A slurry of Pt/C catalyst powder and polytetrafluoroethylene (PTFE, Polyflon D-2CE, Daikin Ind., Japan) in water, prepared by ultrasonic treatment, was spread on a carbon paper (EC-TP1-060T, thickness: 190 μm, Toray Industries, Japan) and then sintered in a 1% H_2/99% Ar atmosphere at 360 °C over 2 h. Pt loading onto the resultant Pt/C electrodes was 2 mg cm^{-2}. The single cell was fabricated with the Pt/C electrodes and pelletized CsH_2PO_4/SiO_2 composite electrolytes (SiO_2: 1 wt%). To enhance mechanical stability, SiO_2 powder (AZ-204, Nippon Silica Industrial, Japan) was added to CsH_2PO_4 (Soekawa Chemicals, Japan) to make a CsH_2PO_4/SiO_2 composite electrolyte by the evaporation-to-dryness method [20]. The prepared composite powder was pressed uniaxially at 4 t cm^{-2} to form a solid electrolyte pellet (diameter: 20 mm; thickness: ca. 1 mm). Pt/C electrodes infiltrated with a saturated CsH_2PO_4 solution were attached to both sides of the electrolyte pellet as working and counter electrodes on a hot plate heated at 150 °C. The geometric area of both working and counter electrodes was 0.57 cm^{-2}. A reference electrode (Pt/C) was also attached to the side of the counter electrode.

2.2. Electrochemical measurement with reaction products analysis

Electrochemical measurements combined with reaction product analyses were performed. The single cell was set in a Pyrex glass tube, which was placed in a thermostatic chamber, and a gaseous mixture of glycerol (purity > 99.0%, Wako Pure Chemical Industries, Ltd., Japan), H_2O (Milli-Q water) and Ar (purity > 99.99%) (typical molar ratio = 1:80:19 for glycerol:water:Ar) was fed into the working electrode side. Glycerol solution was supplied by a microsyringe feeder. The feed solution was vaporized and mixed with Ar in a vaporizer and then supplied continuously to the working electrode. A typical flow rate was 32 ml min^{-1} (sccm). A gaseous mixture of H_2 and H_2O (molar ratio = 49:51) was fed into the counter and reference electrodes side. The influence of hydrogen leakage from the counter electrode side to the working electrode side was confirmed to be negligible through an electrochemical method, the detail of which is described elsewhere [14]. Humidification was also necessary to prevent dehydration of the CsH_2PO_4 [21]. The electrode potentials in this study were defined with respect to the reversible hydrogen electrode (RHE) and were *iR*-corrected. The potentials of the reference electrode were referenced to the RHE with 1 atm of hydrogen (i.e., 0 V *vs*. RHE, conditions: 1 atm of hydrogen at operating temperature). The resistance of each solid electrolyte was evaluated by alternating current (ac) impedance spectroscopic measurements at 1 kHz to correct for the *iR*-loss. Electrochemical measurements with a three-electrode system were conducted using Autolab PGSTAT 30 with a frequency response analyzer module, FRA2 (Eco Chemie B. V., Netherlands). Cyclic voltammetry was conducted at a sweep rate of 1 mV s^{-1}.

A reaction products analysis of glycerol electro-oxidation was conducted with constant anodic polarizations under steady state conditions. Gaseous and liquid products were separated with a cold trap. The gaseous products were then analyzed with a gas chromatograph, GC-8A (Shimadzu Co., Japan), equipped with a thermal conductivity detector (TCD) and a packed column, Shincarbon ST (Shinwa Chemical Ind., Japan). The liquid products were analyzed with a liquid chromatograph (LC-10A, Shimadzu Co.) equipped with a refractive index detector (RID-10A, Shimadzu Co.), a UV detector (SPD-10A, Shimadzu Co.) and cation exchange resin columns, ULTRON PS-80H (Shinwa Chemical Ind.) and Shim-pack SCR-102H (Shimadzu GLC Ltd.).

3. Results and discussion

3.1. Oxidation current during glycerol electro-oxidation at intermediate temperatures

The electro-oxidation of glycerol on a Pt/C electrode at intermediate temperatures was investigated by cyclic voltammetry. Fig. 1a shows a cyclic voltammogram (CV) for the electro-oxidation of glycerol at 250 °C. As references, CV curves of the electro-oxidation of ethanol and ethylene glycol are also plotted in Fig. 1b and c [14,15], as measured by the same method as in this study. The result that the oxidation currents on the forward and backward potential sweeps were almost comparable suggests that the CV measurements for glycerol oxidation were conducted under a quasi-steady state condition. In this study, we subsequently used a sweep rate of 1 mV s^{-1} to obtain a quasi-steady state condition for the evaluation of reaction kinetics during glycerol electro-

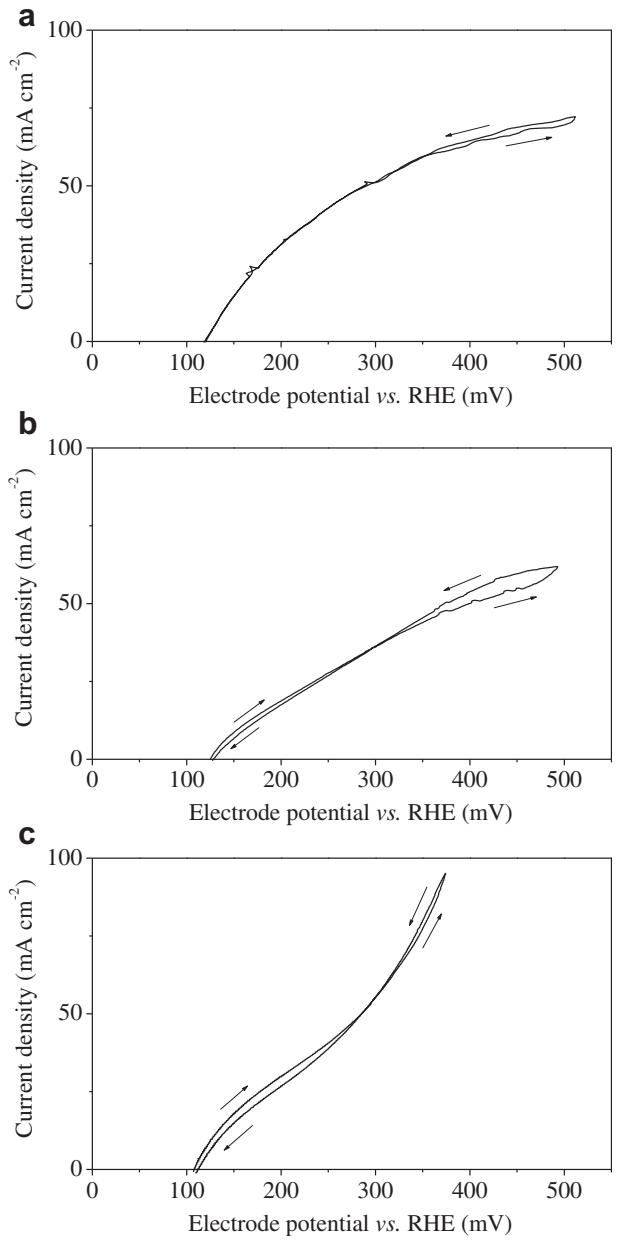

Fig. 1. Cyclic voltammograms for the electro-oxidation of alcohols on a Pt/C electrode at 250 °C (*iR*-corrected). (a): Glycerol; (b): Ethanol; (c): Ethylene glycol. Glycerol (1 mol %)/water (80 mol%)/Ar (19 mol%); ethanol (13 mol%)/water (40 mol%)/Ar (47 mol%) [14]; ethylene glycol (10 mol%)/water (40 mol%)/Ar (50 mol%) [15]; sweep rate: 1 mV s^{-1}.

oxidation. As shown in Fig. 1a, the onset potential of glycerol electro-oxidation was observed at around 120 mV, which was significantly reduced compared with that operated at around room temperature in an acidic medium and even in an alkaline medium (onset potential > 500 mV) [3,6]. This result is favorable in terms of decreasing the overpotential for DAFC operation and resembles the behaviors for ethanol and ethylene glycol electro-oxidation [14,15]. In addition, current density for glycerol electro-oxidation was comparable to or exceeded those for ethanol and ethylene glycol in the low electrode potential region (120–300 mV), despite the low glycerol concentration (1 mol%) compared with those of ethanol (13 mol%) and ethylene glycol (10 mol%) fuels in gaseous mixtures. This result clearly indicates that glycerol electro-oxidation has a high activity on the Pt electrode at intermediate temperatures. At high electrode potentials (300–500 mV), gradual saturation of current density for glycerol electro-oxidation was observed with an increase in electrode potential. Similar behavior was observed during ethanol electro-oxidation [15]. One of possible reasons for the saturation of oxidation current may be high coverage of adsorbed OH formed by dissociative adsorption of water onto the Pt surface.

3.2. Durability of Pt/C electrode toward glycerol electro-oxidation

It has been reported that glycerol can be converted into valuable chemicals through a series of reactions involving dehydration, cracking, and hydrogen transfer with an acid catalyst, wherein acrolein, short olefins, aromatics, acetaldehyde, hydroxyacetone, acids, and acetone were formed through a complex reaction network [22]. The formation of oligomers, olefins, aromatics and subsequent coking may also have led to catalyst degradation in this study. To investigate glycerol electro-oxidation in detail, guaranteed electrode durability should be achieved. Fig. 2 shows the stability of current density with elapsed time for two steam to carbon ratios (S/C = 13 and 27) during glycerol electro-oxidation at 250 °C. When a S/C ratio of 13 was selected, a rapid decrease in the oxidation current for the glycerol electro-oxidation was observed and afterward, the color of the working electrode and its circumference had changed to black or dark brown. A possible reason for the degradation may be the formation of oligomers and subsequent coking. On the other hand, when the higher S/C ratio was selected (S/C = 27), degradation in the current density was

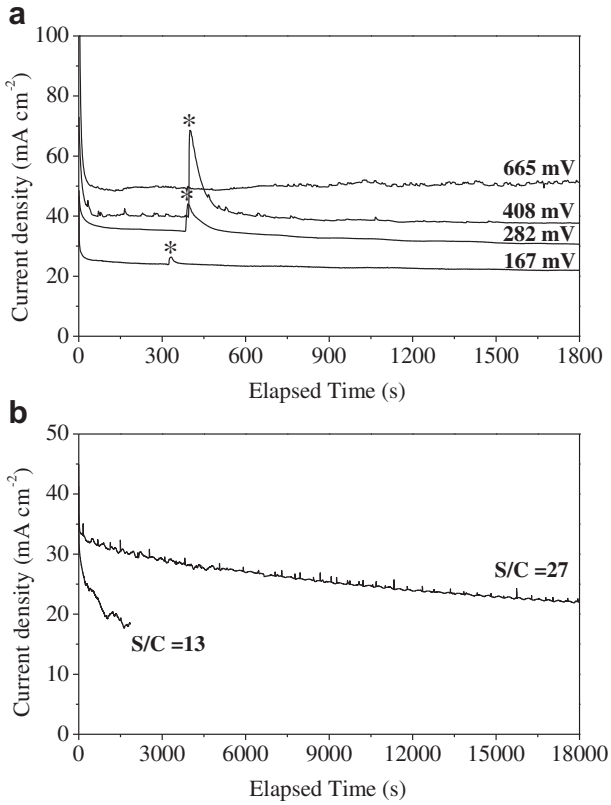

Fig. 2. Variation of current density with time during glycerol electro-oxidation at 250 °C. (a) Short term stability at different potentials with a constant steam to carbon ratio (S/C = 27). (b) Long term stability with different steam to carbon ratios (S/C = 13 (409 mV) and 27 (345 mV)). Marked points by asterisk (*) in Fig. 2a indicate the time when a sampling bag was set up to a gas line to collect gaseous products (i.e., the setting of a sampling bag caused a noise of measured current density).

suppressed. A stable current density was observed at all tested potentials, as shown in Fig. 2. In a further long-term stability test at 550 mV, the degradation rates in current density were ca. 20% for 2 h, and ca. 30% for 5 h. A high S/C ratio may generate OH on Pt and suppress the formation of oligomers, olefins, aromatics and subsequent coking, which results in a relaxation of the degradation of the Pt/C catalyst. To evaluate the initial catalytic activity of the Pt/C electrode, all subsequent experiments were conducted at a S/C ratio of 27.

3.3. Reaction products analysis in glycerol electro-oxidation at intermediate temperature

Reaction products analysis was conducted under steady state polarization conditions at 250 °C. Detected reaction products of C1, C2 and C3 compounds are summarized in Table 1. Main reaction products were C1 products: CO_2, CO, CH_4; C2 products: C_2H_6 and glycolic acid ($HOCH_2COOH$) and H_2. All C3 products were detected as minor components. Fig. 3a and b show concentrations of the main reaction products defined as follows: product (i)/ $\sum$(products + glycerol + water + argon) and the corresponding oxidation current density is plotted in Fig. 3c. It should be noted that conversion of glycerol estimated from reaction products was less than 20%. In this study, observations of glycerol oxidation current were conducted under a low glycerol conversion of around 10–15% with a typical flow rate of 32 ml min^{-1} (sccm) in the working electrode.

As shown in Fig. 3a, a high concentration of CO_2 was detected at all electrode potentials and the CO_2 concentration increased with increasing electrode potential. On the other hand, low concentrations of CO and CH_4 were detected. These results are in contrast to the results found in ethanol and ethylene glycol electro-oxidation, in which high concentrations of CH_4 or CO were detected in the reaction products [14,15]. The oxidation of one glycerol molecule to CO_2 yields 14 electrons, while oxidation to CO yields only 8 electrons. Furthermore, the formation of CH_4 incorporates hydrogen atoms and it is not easily oxidized once it is formed at intermediate temperature. Therefore, a high selectivity for CO_2 in glycerol electro-oxidation is favorable in terms of the effective use of glycerol as a fuel. Although glycolic acid and C_2H_6 were detected as major reaction products, their concentrations were relatively low, especially at each tested electrode potential, except for the rest potential. Furthermore, the concentrations of C3 compounds were lower by over one order of magnitude (<1/10) than the C1 reaction products. These results suggest that rapid C–C bond dissociation of glycerol occurs at 250 °C, which results in a high selectivity for C1 compounds.

Table 1
The list of reaction products.

	Hydrogen (H_2)
C1	Carbon dioxide (CO_2)
	Carbon monoxide (CO)
	Methane (CH_4)
C2	Glycolic acid ($HOCH_2COOH$)
	Ethylene glycol ($HOCH_2CH_2OH$)
	Acetic acid (CH_3COOH)
	Ethane (C_2H_6)
	Ethylene (C_2H_4)
C3	Hydroxyacetone (acetol) (CH_3COCH_2OH)
	Propionic acid (CH_3CH_2COOH)
	Acrolein (acrylaldehyde) (CH_2=$CHCHO$)
	Acetone (CH_3COCH_3)
	1,2-Propanediol ($HOCH_2CH(OH)CH_3$)
	Acrylic acid (CH_2=$CHCOOH$)

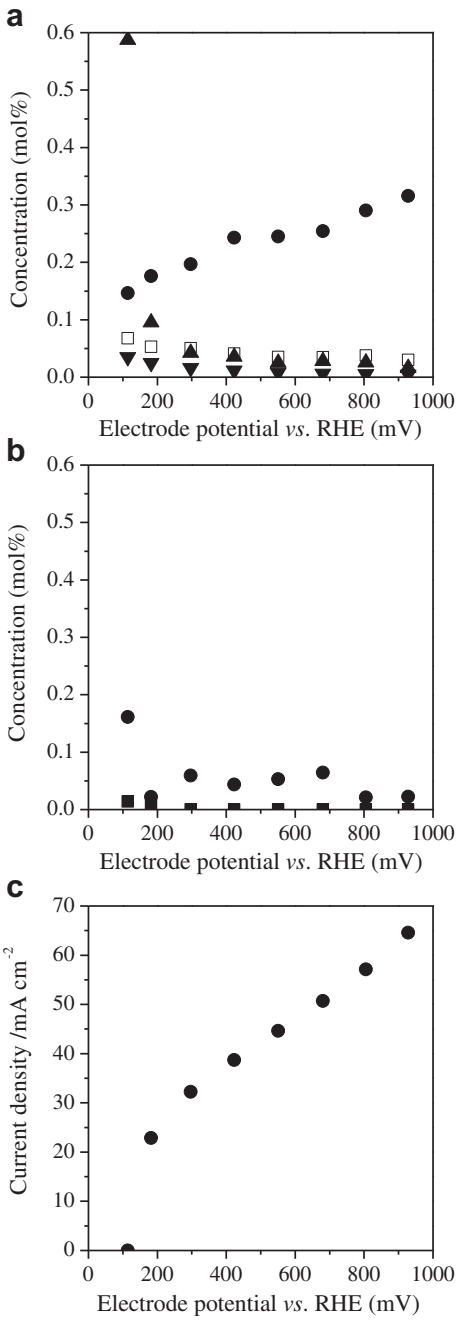

Fig. 3. (a) Concentrations of C1 reaction products and H_2 *vs.* electrode potential for glycerol electro-oxidation under steady state polarization conditions at 250 °C. ▲: H_2; ●: CO_2; □: CO; ▼: CH_4. (b) Concentrations of C2 reaction products *vs.* electrode potential for glycerol electro-oxidation under steady state polarization conditions at 250 °C. ●: Glycolic acid ($HOCH_2COOH$); ■: Ethane (C_2H_6). (c) Corresponding current density *vs.* electrode potential. Glycerol (1 mol%)/water (80 mol%)/Ar (19 mol%); total flow rate: 32 ml min^{-1} (sccm).

It should also be mentioned that, at the rest potential, a large amount of hydrogen was observed as a major product as well as the C1 and C2 main products. This result clearly shows that not only electro-oxidation but also thermal decomposition and steam reforming of glycerol can proceed at intermediate temperatures. A similar result for hydrogen production at the rest potential was observed in our previous studies on ethanol and ethylene glycol electro-oxidation [14,15]. Regarding the dependence of reaction products on electrode potential, only the concentration of CO_2 increased consistently with increasing electrode potential. This

result implies that total oxidation shown in Eq. (1) proceeds with an increase in anodic polarization.

$$C_3H_8O_3 + 3H_2O \rightarrow 3CO_2 + 14H^+ + 14e^- \quad (1)$$

On the other hand, the concentrations of hydrogen and glycolic acid sharply decreased with increased anodic polarization. Additionally, according to their sharp decrease, the oxidation current density in Fig. 3c rose sharply in the low electrode potential region. These observations suggest that at intermediate temperature direct electro-oxidation of glycerol and hydrogen production *via* thermal decomposition and steam reforming of glycerol and subsequent hydrogen oxidation to form proton occur in parallel. Therefore, hydrogen production contributes significantly to the oxidation current, resulting in a high current density even in the low electrode potential region at intermediate temperatures.

To validate the present products analysis, the balance between oxidation current and detected reaction products was investigated as follows. First, the contributions of each reaction product toward current density were estimated (i_{pro}), assuming apparent stoichiometric reactions corresponding to every detected reaction product. The assumed reactions are listed in Table 2. The current densities estimated from every reaction were then summarized (Σi_{pro}). Finally, the value of Σi_{pro} was compared with the current density (I_{elec}) measured by an electrochemical method (i.e., I_{elec} is the same as that in Fig. 3c). The contributions of all reaction products, such as C1, C2, C3 compounds and H_2 (i.e., Σi_{pro}) are plotted against electrode potential in Fig. 4a. Because H_2 is detected as a residual non-oxidized product, it is counted as a negative contribution toward Σi_{pro}. The contribution of C3 reaction products was, however, too small to show in the figure because of their low concentrations. Although Σi_{pro} of C2 products was scattered with respect to electrode potential, the contribution of C1 products was over 60% for Σi_{pro} and increased with increasing electrode potential. In Fig. 4b, Σi_{pro} and I_{elec} are plotted against electrode potential. Σi_{pro} is mostly comparable to I_{elec}, which suggests that most of the I_{elec} originated from the detected reaction products. Slight differences between Σi_{pro} and I_{elec} were observed at low potentials (300–500 mV), which may be derived from the accuracy of C1 and C2 product quantities.

Fig. 5 shows the selectivity of C1, C2 and C3 reaction products based on the number of carbon atoms. Selectivity, S_n, was thus defined as follows:

$$S_n = \frac{nC_{Cn}}{C_{C1} + 2C_{C2} + 3C_{C3}} \times 100 \quad (n = 1, 2, 3) \quad (2)$$

where C_{C1}, C_{C2}, C_{C3}, and n are the concentrations of C1, C2, C3 reaction products and the number of carbon atoms in the reaction

Table 2
The list of stoichiometric reaction equations based on detected reaction products.

<1>	$C_3H_8O_3 + 3H_2O \rightarrow 7H_2 + 3CO_2$
<2>	$C_3H_8O_3 \rightarrow 4H_2 + 3CO$
<3>	$C_3H_8O_3 + 5H_2 \rightarrow 3CH_4 + 3H_2O$
<4>	$C_3H_8O_3 + 3.5H_2 \rightarrow 1.5C_2H_6 + 3H_2O$
<5>	$C_3H_8O_3 + 2H_2O \rightarrow HOCH_2COOH + CO_2 + 4H_2$
<6>	$C_3H_8O_3 + 2H_2 \rightarrow 1.5C_2H_4 + 3H_2O$
<7>	$C_3H_8O_3 \rightarrow 1.5CH_3COOH + 2H_2$
<8>	$C_3H_8O_3 + 0.5H_2 \rightarrow 1.5HOCH_2CH_2OH$
<9>	$C_3H_8O_3 + H_2 \rightarrow HOCH_2CH(OH)CH_3 + H_2O$
<10>	$C_3H_8O_3 \rightarrow CH_3COCH_2OH + H_2O$
<11>	$C_3H_8O_3 \rightarrow CH_3CH_2COOH + H_2O$
<12>	$C_3H_8O_3 \rightarrow CH_2{=}CHCOOH + H_2 + H_2O$
<13>	$C_3H_8O_3 + H_2 \rightarrow CH_3COCH_3 + 2H_2O$
<14>	$C_3H_8O_3 \rightarrow CH_2{=}CHCHO + 2H_2O$

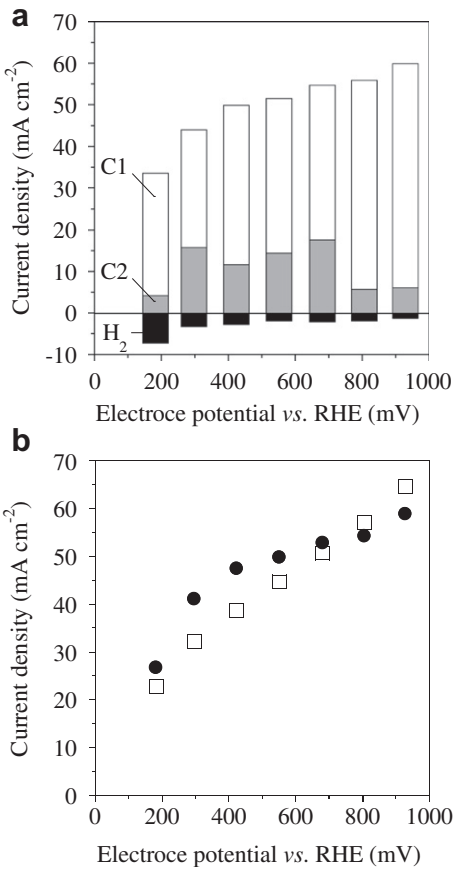

Fig. 4. (a) Contributions of C1, C2, C3 compounds and H_2 to current density (Σi_{pro}) *vs.* electrode potential. White bar: C1 products; gray bar: C2 products; black bar: H_2. (b) Comparison of Σi_{pro} with I_{elec}. ●: Σi_{pro}; □: I_{elec}. Experimental conditions were the same as in Fig. 3.

products, respectively. The selectivity of C2 products decreased with an increase in electrode potential, while that of C1 products increased with an increase in electrode potential and reached a value of around 80% in the high electrode potential region. The selectivity of C3 compounds was very low at all tested electrode potentials. These results clearly show the high activity of the Pt/C electrode toward C–C bond dissociation at intermediate

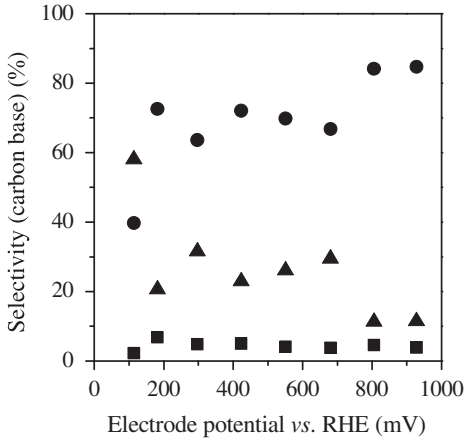

Fig. 5. Selectivity for C1, C2 and C3 reaction products for glycerol electro-oxidation under steady state polarization conditions at 250 °C. ●: C1; ▲: C2; ■: C3. Experimental conditions were the same as in Fig. 3.

temperatures. The ratio of C–C bond dissociation was estimated by the following definition of Eq. (3).

$$S_{c-c} = \frac{C2 + 2/3(C1 - C2)}{2/3(C1 + 2C2 + 3C3)} = \frac{(M_1 + 0.25M_2)}{M_{all}} \quad (3)$$

where M_1, M_2, M_{all} are, respectively, the sum of the carbon numbers in C1 products, C2 products and the summation of carbon number in all reaction products C1, C2 and C3. As shown in Fig. 6, high ratios of C–C bond dissociation were obtained at all electrode potentials. As mentioned in the Introduction, at relatively low temperatures, a low CO_2 current efficiency (3–5% at around 600–700 mV) was reported [6]. This suggests that the slow oxidation kinetics of glycerol is due to a high barrier of C–C bond dissociation. On the other hand, the C–C bond dissociation ratio reached 70–80%, at both low and high potentials (>200 mV) at 250 °C. This result suggests that the C–C bond dissociation of adsorbed C3 compounds is accelerated through an increase in operating temperature, resulting in a high selectivity for C1 and C2 reaction products, which consequently leads to the efficient use of glycerol fuel in DAFCs.

3.4. Reaction kinetics in glycerol electro-oxidation on a Pt/C electrode at intermediate temperatures

To further understand the reaction mechanism in glycerol electro-oxidation at around 250 °C, the dependence of oxidation current on flow rate was investigated. Cyclic voltammograms performed with different flow rates between 32 and 128 ml min^{-1} (sccm) are shown in Fig. 7. With an increase in flow rate, the rest potential (i.e., onset potential) shifted to the positive side and the current density decreased, especially in the low and middle electrode potential region (120–400 mV). In addition, with higher flow rate, lower concentration of hydrogen production was observed. These results suggest that the current density is strongly influenced by the amount of hydrogen production *via* thermal decomposition and steam reforming of glycerol. Therefore, the behavior of CV curves in Fig. 7 can support a parallel reaction route mechanism between hydrogen production (indirect route) and direct electro-oxidation of glycerol (direct route), as mentioned above. At potentials higher than 400 mV, the CV curves mostly become comparable despite differences in flow rate, suggesting that the direct electro-oxidation becomes dominant at high potentials. In

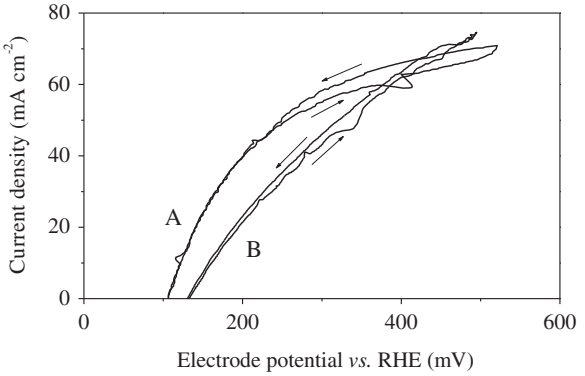

Fig. 7. Cyclic voltammograms of glycerol electro-oxidation on Pt/C performed with different total flow rates at 250 °C. Curve A: 32 ml min^{-1} (sccm); curve B: 128 ml min^{-1} (sccm). Glycerol (1 mol%)/water (80 mol%)/Ar (19 mol%); sweep rate: 1 mV s^{-1}.

conclusion, the results presented in Figs. 3–7 are mainly explained by the parallel reaction route mechanism (Eq. (4)).

$$C_3H_8O_3 \xrightarrow{\text{Indirect}} H_2 + Cn(n = 1-3) \rightarrow 2H^+ + 2e^- + Cn \quad (a)$$

$$\xrightarrow{\text{Direct } (+3H_2O)} 3CO_2 + 14H^+ + 14e^- \quad (b)$$

$$(I_{total} = I_{indirect} + I_{direct}) \quad (4)$$

It should be noted that the proposed mechanism is very similar to our previous studies on ethanol and ethylene glycol electro-oxidation [14,15]. The indirect reaction route (Eq. (4a)) for H_2 oxidation may involves a mass transport process as well as a charge transfer process because the H_2 concentration is very low. The direct reaction route (Eq. (4b)) is described by a charge transfer process for glycerol oxidation.

To evaluate the apparent activation energy of glycerol electro-oxidation, CV measurements were conducted at various temperatures between 235 and 260 °C. Fig. 8 shows the forward potential sweep of cyclic voltammograms performed at different temperatures. Higher current densities were observed with increasing temperature, especially at low and middle electrode potentials (120–500 mV). However, the current densities were saturated and became almost comparable at around 700 mV. This observation may be caused by a high coverage of adsorbed OH on the Pt surface, derived from the dissociation of water at high electrode potentials.

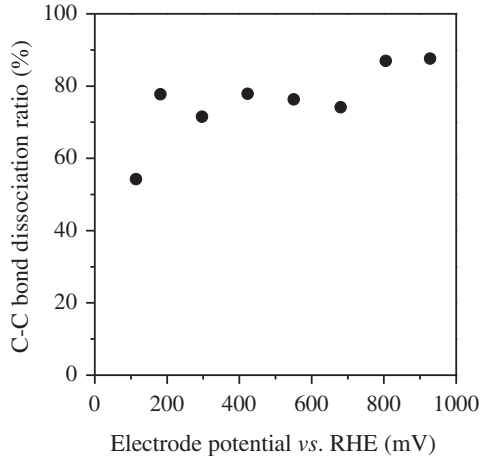

Fig. 6. C–C bond dissociation ratio *vs.* electrode potential. Experimental conditions were the same as in Fig. 3.

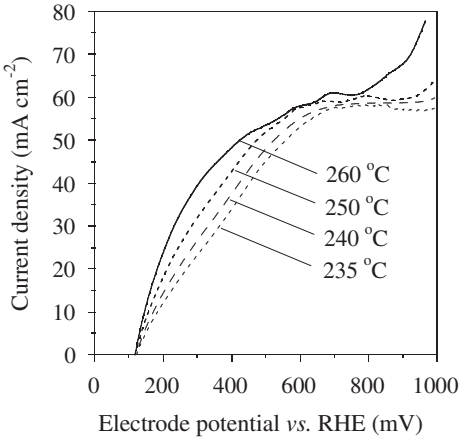

Fig. 8. Cyclic voltammograms of glycerol electro-oxidation on Pt/C at different temperatures (*iR*-corrected). CV curves for forward potential sweep are shown in the figure. Glycerol (1 mol%)/water (80 mol%)/Ar (19 mol%); total flow rate: 32 ml min^{-1} (sccm); sweep rate: 1 mV s^{-1}.

Generated OH prevents glycerol from adsorbing on the Pt to reduce the oxidation current at high electrode potentials.

Arrhenius plots for the current densities at various electrode potentials below 500 mV are shown in Fig. 9a. Linearity between the natural logarithm of the current density, ln *i*, and the inverse of reaction temperature was observed at these electrode potentials. If we assume that the reaction proceeds according to the Butler–Volmer equation (Eq. (5)) for anodic current, the apparent activation energy, E_a, for each electrode potential, *E*, is represented by Eq. (6).

$$i = nFA\exp\left(-\frac{E_{a,0}}{RT}\right)\exp\left(\frac{(1-\alpha)nFE}{RT}\right) \quad (5)$$

$$E_a = -R\left(\frac{\partial \ln i}{\partial(1/T)}\right)_E = E_{a,0} - (1-\alpha)nFE \quad (6)$$

where *n*, *F*, *A*, α and *R* are electron transfer number, Faraday constant, pre-exponential factor, transfer coefficient and gas constant, respectively. Thus, Eq. (6) suggests a linear relationship between E_a and *E* with the slope of $-(1-\alpha)nF$, if the rate-determining step involves a charge transfer reaction.

The apparent activation energies evaluated from each slope of the Arrhenius plots using Eq. (6) are shown in Fig. 9b. Accuracy for E_a was also estimated by considering the degradation of glycerol electro-oxidation on the Pt/C electrode. As shown in Fig. 9b, the apparent activation energy decreased from 70 to 20 kJ mol^{-1} with an increase in electrode potential from 150 to 500 mV, which shows a linear relationship with the electrode potential. For reference, the E_a of ethylene glycol (C2 polyalcohol) evaluated at intermediate temperatures is also plotted in Fig. 9b, which was recalculated by Eq. (6) using the data in the literature [15]. The dependence of E_a on electrode potential for glycerol and ethylene glycol is contrary to this result, i.e., the former has a linear relationship with electrode potential, while the latter is mostly independent on electrode potential. The rate-determining step in ethylene glycol electro-oxidation may involve a potential independent step such as C–C (or C–H) bond dissociation during early reaction steps. On the other hand, the rate-determining step in glycerol electro-oxidation should involve a potential-dependent step. The reaction products analysis shows that C3 reaction products were minor, suggesting that C–C bond dissociation of glycerol during early reaction steps can proceed rapidly on Pt/C. Possible reactions dependent on the electrode potential are hydrogen oxidation ($H_2 \rightarrow 2H^+ + 2e^-$) and OH formation from water ($H_2O \rightarrow OH_{ads} + H^+ + e^-$) but the former is generally a rapid process. Considering the above, subsequent oxidation of intermediate species by OH, followed by the C–C bond dissociation of glycerol, is plausible as a rate-determining step. A more detailed reaction route is discussed below.

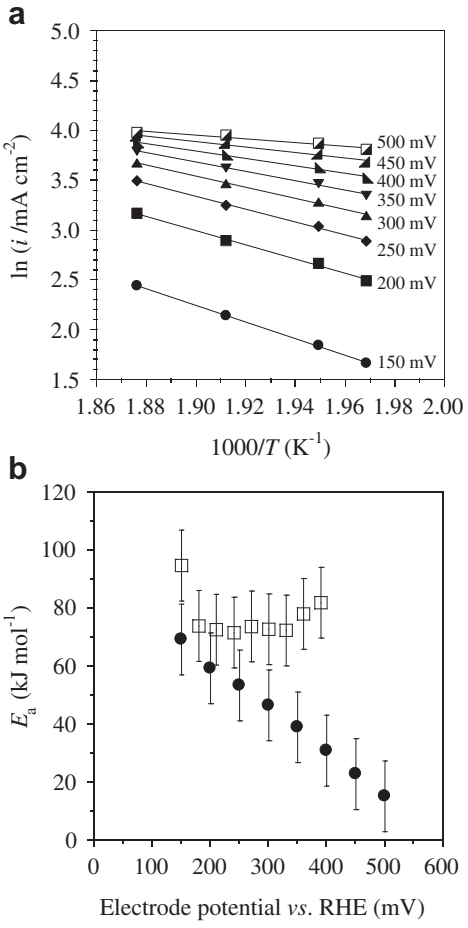

Fig. 9. (a) Arrhenius plots for current densities for glycerol electro-oxidation at different electrode potentials. (b) Apparent activation energies in electro-oxidation of glycerol (●) and ethylene glycol (□) *vs.* electrode potential.

3.5. Reaction mechanism of glycerol electro-oxidation on a Pt/C electrode at intermediate temperatures

It was found that both hydrogen production and direct electro-oxidation of glycerol proceeded in parallel. Furthermore, both high CO_2 selectivity and low CO and CH_4 selectivity were observed. In this section, the reaction mechanism of glycerol electro-oxidation is discussed in detail. According to the current results and previous reports, including density functional theory (DFT) calculation for glycerol decomposition on a Pt surface [3,5,9,23], a schematic reaction mechanism at intermediate temperature is proposed in Fig. 10, in which the main and sub-reaction paths are described. The main reaction path involves the formation of C1 products and the sub-reaction path involves the formation of C2 and C3 products. According to the DFT calculation previously reported [23], the activation energy for C–C bond dissociation is higher than that of C–H bond dissociation for glycerol and for intermediates ($(CH_xO_yH_z)_{3,ads}$) during the early stage of dehydrogenation. On the other hand, after the removal of several hydrogen atoms from the intermediates (C–H bond dissociation of $(CH_xO_yH_z)_{3,ads}$), the activation energies for both C–H and C–C bond dissociations become comparable. Therefore, as shown in Fig. 10, on the Pt surface, C–H bond dissociation may proceed rapidly (reaction 2), and then C–C bond dissociation occurs to form $(CH_xO_yH_z)_{2,ads}$ and $CH_xO_yH_{z,ads}$ (reactions 3 and 3′). Because methanol and formic acid were not detected in this study, the oxidation of $CH_xO_yH_{z,ads}$, which may have a similar molecular structure to an intermediate in the oxidation of methanol, will rapidly proceed and then form CO_2 as a major reaction product *via* oxidation of CO_{ads} by OH_{ads} (reactions 7 and 9). Because the S/C ratio was high (S/C = 27) in this study, adsorbed CO could easily be oxidized to CO_2 and thus very high CO_2 selectivity was achieved under the present condition.

Meanwhile, part of the $C3_{ads}$ may react *via* dehydration, hydrogenolysis and dehydrogenation to convert to other $C3_{ads}$ intermediate species (reactions 11, 12 and 13), and then desorb to form C3 compounds such as hydroxyacetone (acetol), propionic acid, acrolein, acetone, 1,2-propanediol and acrylic acid. However, those selectivities were very low, because rapid C–C bond dissociation occurs at intermediate temperatures. As for the formation of C2 compounds, if just one C–C bond dissociation of glycerol proceeds to form $C2_{ads}$ intermediate species (reaction 3′), C2 compounds such as glycolic acid, ethylene glycol, acetic acid, C_2H_6 and C_2H_4 can be generated (reactions 15–20).

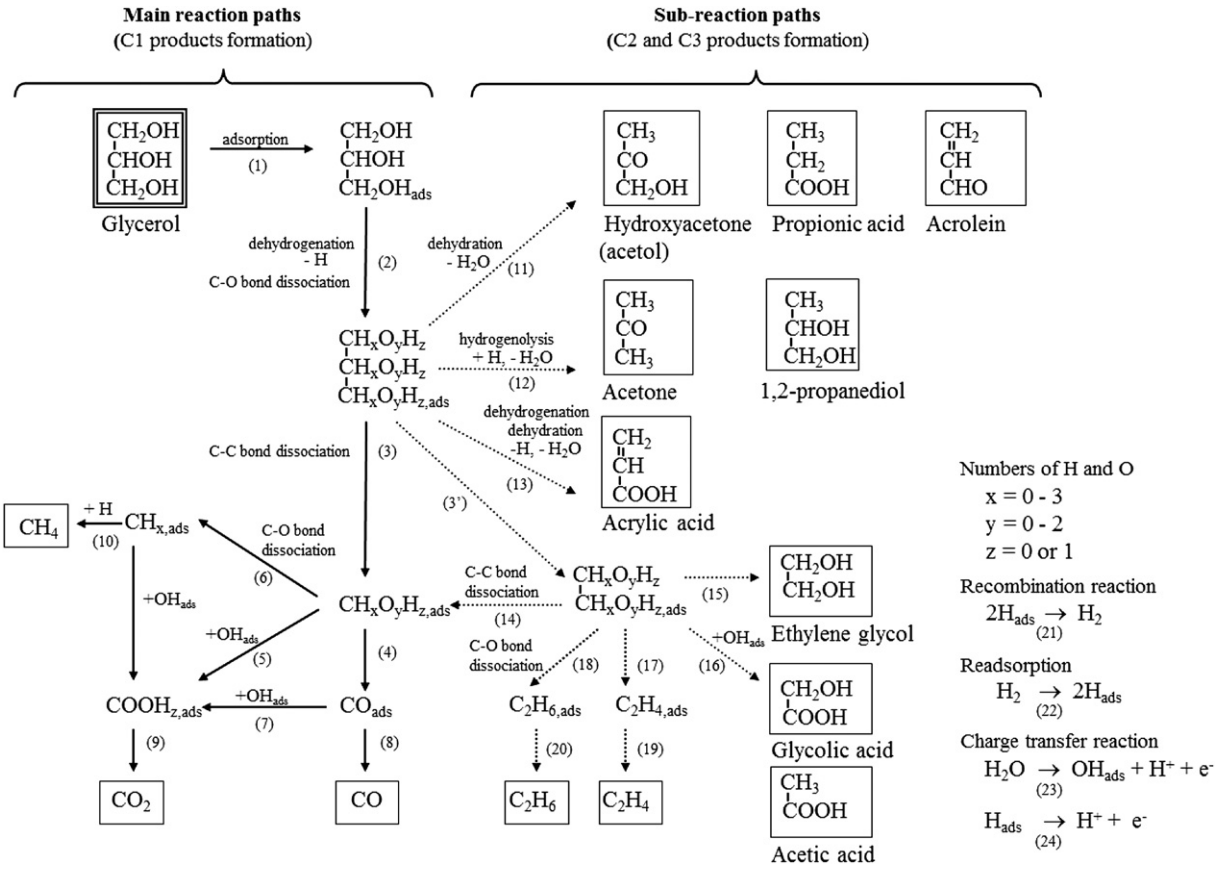

Fig. 10. Proposed reaction mechanism for glycerol electro-oxidation on a Pt/C electrode at intermediate temperature. Reaction products detected in this study are surrounded by squares. Solid arrows: main reaction paths; dotted arrows: sub-reaction paths.

H_2 forms *via* recombination of H_{ads} (reaction 21), which is mainly generated *via* dehydrogenation of glycerol (reaction 2). Part of the H_2 adsorbs onto Pt again (reaction 22) and is oxidized to form protons (H^+). For the charge transfer reaction, dissociative adsorption of water to form OH_{ads} and oxidation of adsorbed H atoms to form H^+ are considered (reactions 23 and 24).

For the efficient use of fuel, high C1 selectivity and low C2 and C3 selectivity are required. In addition, high CO_2 selectivity and low CO and CH_4 selectivity in C1 products are desirable. To achieve high selectivity of CO_2, acceleration of C–C bond dissociation (reaction 3), rapid oxidation of intermediates by adsorbed OH (reactions 5 and 7), and suppression of C–O bond dissociation (reactions 6, 11–13, 17, 18) are necessary. In this study, a high selectivity for CO_2 and low selectivity for CO and CH_4 in glycerol electro-oxidation were observed. This result suggests that C–C bond dissociation proceeded rapidly but C–O bond dissociation was adequately suppressed during the present glycerol electro-oxidation. Therefore, a high carbon to oxygen (C/O) ratio in a molecule is also useful for fuel to realize high CO_2 selectivity. This view agrees with the results in ethanol and ethylene glycol electro-oxidation at intermediate temperatures [14,15]. The present study, however, indicates that stable electro-oxidation of glycerol requires a very high S/C ratio (S/C = 27). In the electro-oxidation of ethylene glycol, a relatively high selectivity for CO was observed when the S/C ratio was not high (S/C = 1–2). Therefore, high CO_2 selectivity and low CO selectivity in the glycerol electro-oxidation may be achieved by a high S/C ratio. To achieve further improvements in glycerol electro-oxidation, investigation of the reaction mechanism at low S/C ratios and mitigation of the degradation of catalyst should be carried out.

4. Conclusions

Glycerol electro-oxidation on the Pt/C electrode was conducted at intermediate temperatures (235–260 °C) in combination with a reaction products analysis. Through the measurements, the following results and conclusions were derived: (1) A high oxidation current during glycerol electro-oxidation was observed even at a dilute glycerol concentration (1 mol%), which is roughly comparable to those measured in the electro-oxidation of C2 alcohols such as ethanol (13 mol%) and ethylene glycol (10 mol%). (2) Stable operation during glycerol electro-oxidation at around 250 °C requires a high S/C ratio (e.g., S/C = 27). Under a low S/C condition, rapid degradation of Pt/C electrode performance and a change in color of the electrode surface were observed. (3) Hydrogen production *via* thermal decomposition and steam reforming of glycerol (indirect path) and direct electro-oxidation of glycerol (direct path) proceed in parallel and both the reactions contribute to total oxidation current. (4) The main reaction products were C1 products: CO_2, CO, CH_4; C2 products: C_2H_6 and glycolic acid ($HOCH_2COOH$) and H_2. All C3 products were detected at minor levels. The products analysis also shows that total oxidation (i.e., CO_2 formation) can proceed smoothly at the intermediate temperature. (5) C–C bond dissociation ratio reached 70–80% at both low and high potentials (>200 mV) at 250 °C and the selectivity for C1 products (CO_2, CO and CH_4) increased with increasing electrode potential and reached a value of around 80% in the high electrode potential region. (6) The apparent activation energy for the direct electro-oxidation of ethylene glycol was 70–20 kJ mol^{-1} at electrode potentials between 150 and 500 mV. A linear relationship between

activation energy and electrode potential suggests that the rate-determining step in glycerol electro-oxidation involves a potential-dependent step. One possible rate-determining step is the oxidation step of intermediate species formed after C–C bond dissociation of glycerol by adsorbed OH. These observations provide new insights into the polyol oxidation mechanism and suggest strategies for the effective operation of DAFCs.

Acknowledgments

This work was financially supported by a Jiro Kondo Grant from the Asahi Glass Foundation and a Grant-in-Aid for Young Scientists (A), no. 20681007, from the Ministry of Education, Culture, Sports, Science, and Technology of Japan, both of which are greatly appreciated.

References

[1] C.-H. Zhou, J.N. Beltramini, Y.-X. Fan, G.Q. Lu, Chem. Soc. Rev. 37 (2008) 527–549.
[2] J. Xuan, M.K.H. Leung, D.Y.C. Leung, M. Ni, Renew. Sustain. Energy Rev. 13 (2009) 1301–1313.
[3] L. Roquest, E.M. Belgsir, J.-M. Lbger, C. Lamy, Electrochim. Acta 39 (16) (1994) 2387–2394.
[4] E.C. Venancio, W.T. Napporn, A.J. Motheo, Electrochim. Acta 47 (2002) 1495–1501.
[5] S. Kongjao, S. Damronglerd, M. Hunsom, J. Appl. Electrochem. 41 (2011) 215–222.
[6] J. Schnaidt, M. Heinen, D. Denot, Z. Jusys, R.J. Behm, J. Electroanal. Chem. 661 (2011) 250–264.
[7] C.A. Martins, M.J. Giz, G.A. Camara, Electrochim. Acta 56 (2011) 4549–4553.
[8] A.N. Grace, K. Pandian, Electrochem. Commun. 8 (2006) 1340–1348.
[9] J.F. Gomes, G. Tremiliosi-Filho, Electrocatalysis 2 (2011) 96–105.
[10] M. Schell, Y. Xu, Z. Zdraveski, J. Phys. Chem. 100 (1996) 18962–18969.
[11] V. Bambagioni, C. Bianchini, A. Marchionni, J. Filippi, F. Vizzaa, J. Teddy, Philippe Serp, M. Zhiani, J. Power Sources 190 (2009) 241–251.
[12] M. Avramov-Ivic, J.-M. Leger, B. Beden, F. Hahn, C. Lamy, J. Electroanal. Chem. 351 (1993) 285–297.
[13] A. Falase, K. Garcia, C. Lau, P. Atanassov, Electrochem. Commun. 13 (2011) 1488–1491.
[14] I. Shimada, Y. Oshima, J. Otomo, J. Electrochem. Soc. 158 (2001) B369–B375.
[15] F. Kosaka, Y. Oshima, J. Otomo, Electrochim. Acta 56 (2011) 10093–10100.
[16] A.I. Baranov, V.P. Khiznichenko, V.A. Sandler, L.A. Shuvalov, Ferroelectrics 81 (1988) 183–186.
[17] J. Otomo, N. Minagawa, C.-J. Wen, K. Eguchi, H. Takahashi, Solid State Ionics 156 (2003) 357–369.
[18] D.A. Boysen, S.M. Haile, H. Liu, R.A. Secco, Chem. Mater. 15 (2003) 727–736.
[19] J. Otomo, S. Nishida, H. Takahashi, H. Nagamoto, J. Electroanal. Chem. 615 (2008) 84–90.
[20] H. Shigeoka, J. Otomo, C.-J. Wen, M. Ogura, H. Takahashi, J. Electrochem. Soc. 151 (2004) J76–J83.
[21] J. Otomo, T. Tamaki, S. Nishida, S. Wang, M. Ogura, T. Kobayashi, C.-J. Wen, H. Nagamoto, H. Takahashi, J. Appl. Electrochem. 35 (2005) 865–870.
[22] A. Corma, G.W. Huber, L. Sauvanaud, P. O'Connor, J. Catal. 257 (2008) 163–171.
[23] B. Liu, J. Greeley, J. Phys. Chem. C 115 (2011) 19702–19709.